ChemPubSoc Europe

DOI: 10.1002/chem.201501863

CHEMISTRY A European Journal Full Paper

Photochemistry

Ultrafast Spectroscopy of Hydroxy-Substituted Azobenzenes in Water

Sabrina Steinwand,[a] Thomas Halbritter,[b] Dominique Rastädter,[c] Juan Manuel Ortiz-Sánchez,[c] Irene Burghardt,*[c] Alexander Heckel,*[b] and Josef Wachtveitl*[a]

Abstract: Ultrafast UV/Vis pump/probe experiments on *ortho*-, *meta*- and *para*-hydroxy-substituted azobenzenes (HO-ABs), as well as for sulfasalazine, an AB-based drug, were performed in aqueous solution. For *meta*-HO-AB, AB-like isomerisation behaviour can be observed, whereas, for *ortho*-HO-AB, fast proton transfer occurs, resulting in an excited keto species. For *para*-HO-AB, considerable keto/enol tautomerism proceeds in the ground state, so after excitation the *trans*-keto species isomerises into the *cis* form. Aided by TD-DFT calculations, insight is provided into different deactivation pathways for HO-AB, and reveals the role of hydroxy groups in the photochemistry of ABs, as well as their acetylation regarding sulfasalazine. Hydroxy groups are position-specific substituents for AB, which allow tuning of the timescale of thermal relaxation, as well as the amount and contribution of the keto species to photochemical processes.

Introduction

In recent years, photochromic molecules, which have the ability to undergo reversible structural changes after activation by light, have become increasingly important for a wide field of applications, ranging from regulation of biological processes to data storage.[1–4] The photoisomers of these photoswitches differ significantly and changes in their physical and chemical properties can be used to control a variety of biological effects or properties of a material with an external light signal. The use of light has various advantages: no additional chemical components have to be brought into the system, and therefore, possible side reactions and disturbance of the biological system is avoided. Furthermore, irradiation can be performed with a simple experimental setup and spatial and temporal control allows an exact location and timing of the desired effect.

Among the best studied photochromic systems are derivatives of azobenzene (AB), which can be present as either *trans* or *cis* isomers. Irradiation of the *trans* form with UV light typically generates the *cis* isomer, which, in turn, can be switched back to the *trans* isomer with visible-light irradiation or through a thermally controlled pathway.[5,6]

This type of photoswitch is a powerful tool whenever a conformational change should be induced. In this way, AB is used in polymers[7] and foldamers,[8] gold nanoparticles,[9] liquid crystals[4] and even crystals for non-linear optics.[10] Another important field is the biological application of ABs,[11] with contributions from our groups and the groups of Asanuma or Trauner. In AB-modified peptides, a light-dependent modulation of secondary[12,13] and tertiary structural motifs[14] was demonstrated. ABs have also been covalently introduced into DNA and RNA[15] either as hybridisation photoswitches[16] or to modulate the activity of ligand-gated ion channels.[17,18]

In our attempts to develop a light-responsive riboswitch, we are interested in highly functionalised AB-containing small molecules. Investigating the photoswitchability of the commercially available sulfasalazine (**1**; Figure 1), a drug known for the treatment of inflammatory bowel disease and rheumatoid arthritis, we could only detect moderate switching behaviour in anhydrous DMSO. In aqueous environments, however, *trans*–*cis* isomerisation could not be observed by UV/Vis measurements after illumination at $\lambda = 365$ nm. Acetylation of the hydroxy group (**2**) allows accumulation of the *cis* isomer, again on a moderate timescale. A variety of studies have been performed on HO-ABs regarding, for example, pH[19] and solvent dependence,[20,21] as well as fast thermal *cis*–*trans* relaxation.[22,23] One possible reason for the fast relaxation rates is the proposed keto/enol tautomerism of HO-AB, resulting in a ketohydrazone in protic solvents.[24–29] Although *ortho*-HO-ABs could undergo intramolecular proton transfer, *para* substitution should give rise to an intermolecular mechanism

[a] S. Steinwand, Prof. Dr. J. Wachtveitl
Institute of Physical and Theoretical Chemistry
Goethe-University Frankfurt, Max-von-Laue-Str. 7
60438 Frankfurt (Germany)
E-mail: wveitl@theochem.uni-frankfurt.de

[b] T. Halbritter, Prof. Dr. A. Heckel
Institute for Organic Chemistry and Chemical Biology
Goethe-University Frankfurt, Max-von-Laue-Str. 7
60438 Frankfurt (Germany)

[c] D. Rastädter, Dr. J. M. Ortiz-Sánchez, Prof. Dr. I. Burghardt
Institute of Physical and Theoretical Chemistry
Goethe-University Frankfurt, Max-von-Laue-Str. 7
60438 Frankfurt (Germany)

Supporting information for this article is available on the WWW under http://dx.doi.org/10.1002/chem.201501863.

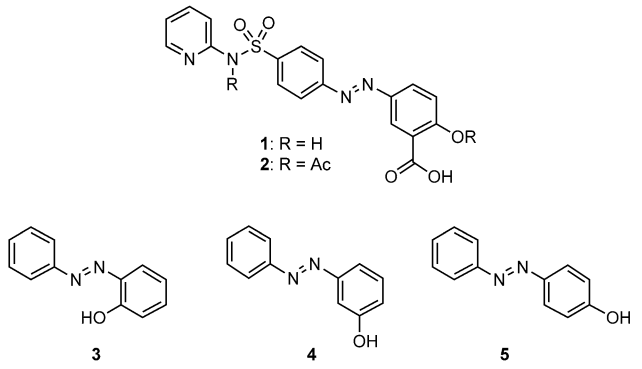

Figure 1. Chemical structures of sulfasalazine (**1**) and its acetylated derivative **2**, as well as the three hydroxy-substituted azobenzenes (HO-ABs; **3**–**5**) investigated herein.

through solvent molecules. However, no ultrafast measurements have been performed so far, so the question arises as to how HO-ABs isomerise (*trans*–*cis*) and if the contribution from a keto species can be detected. Moreover, one needs to investigate if intra-/intermolecular proton transfer occurs in the ground state or only after photoactivation. Therefore, we present herein ultrafast spectroscopic studies of HO-ABs **3**–**5** (Figure 1), in addition to sulfasalazine before (**1**) and after acetylation (**2**). Moreover, DFT and time-dependent (TD) DFT calculations have been carried out to shed light on the complex photochemical scenario outlined above. Our theoretical studies of the potential energy surfaces (PESs) of **3** and **5** for S_0, S_1 and S_2 have been carried out with an implicit water model, in which the molecule is placed inside a cavity of the solvent.

Results and Discussion

Steady-state investigations

Spectral characteristics of compound **1** are highly dependent on the proticity of the solvent. Only about 4% of phosphate-buffered saline (PBS) in a solution of compound **1** in DMSO suffices to induce a considerable blueshift of the absorbance maximum, resulting in a loss of switchability in the steady state (data not shown), whereas isomerisation behaviour can be detected in the range of seconds in DMSO. In detail, compound **1** shows a broad and structured UV/Vis spectrum in anhydrous DMSO (Figure 2). The most intense band at $\lambda =$ 400 nm is assigned to the $\pi\pi^*$ band (S_2 state) of the *trans* isomer, whereas the $n\pi^*$ band (S_1 state) can barely be seen. After illumination at $\lambda = 365$ nm, compound **1** shows sufficiently good switching behaviour in anhydrous DMSO. Whereas the absorption of the $\pi\pi^*$ band of *trans*-AB decreases, the $\pi\pi^*$ band at $\lambda = 327$ nm and the $n\pi^*$ band at $\lambda = 536$ nm of the *cis* isomer increase. The PSS, however, contains only a small amount of *cis* isomer. The thermal back reaction proceeds with a lifetime of $\tau = (24.6 \pm 0.7)$ s. Nevertheless, the addition of only a small amount of PBS shifts the $\pi\pi^*$ band hypsochromically by about 40 nm to $\lambda = 360$ nm; the $n\pi^*$ contribution is now seen at $\lambda \approx 450$ nm. Similar to DMSO, in PBS a structured UV/Vis spectrum is also observed with an additional blueshifted band at $\lambda \approx 320$ nm. However, no spectrum of a PSS can be recorded due to acceleration of the thermal back reaction. In a flash photolysis setup, this thermal relaxation of an aqueous solution of **1** was measured after excitation at $\lambda = 325$ nm. Negative absorption changes were recorded at $\lambda = 365$ nm, corresponding to bleaching of the $\pi\pi^*$ band of *trans*-**1**, which decays with $\tau = (61.3 \pm 0.8)$ ms (see Figures S9 and S10 in the Supporting Information). This fast thermal back reaction, as well as the slight redshift with respect to pure AB ($\lambda_{max}(\pi\pi^*) =$ 314 nm),[30] can be explained by a push–pull effect of the hydroxy and sulfonamide groups of compound **1**; this is, however, weakened by the $-M$ effect of the carboxy group. Acetylation results in a loss of this effect and decelerates the thermal back rate to a timescale of hours. Moreover, the UV/Vis spectrum of the **2**-*trans* isomer is about 32 nm hypsochromically shifted with respect to **1**. The $\pi\pi^*$ band of *trans*-**2** can be seen at $\lambda = 328$ nm with a weak $n\pi^*$ contribution at $\lambda = 435$ nm. This compound can be converted into the PSS spectrum with an increased $n\pi^*$ band at $\lambda = 420$ nm by illumination at $\lambda =$ 365 nm (Figure 2).

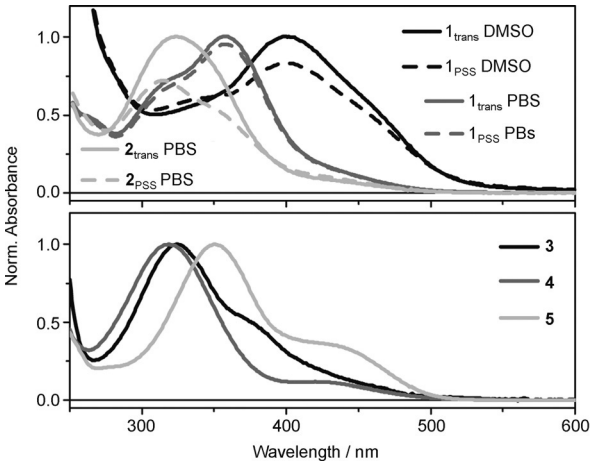

Figure 2. Steady-state UV/Vis spectra of **1** in (anhydrous) DMSO and PBS, and **2** in PBS before (*trans*) and after illumination (photostationary state (PSS)) at $\lambda = 365$ nm (top), as well as spectra of **3**, **4** and **5** at thermal equilibrium in PBS (bottom).

The UV/Vis spectrum of *trans*-**4** shows a narrow $\pi\pi^*$ band at $\lambda = 319$ nm with an $n\pi^*$ band at $\lambda = 420$ nm; for the PSS, an increased $n\pi^*$ band at $\lambda = 425$ nm can be seen (data not shown). The absorption bands of compound **3** are only slightly redshifted to $\lambda = 324$ nm (S_2). However, in contrast to **4**, an additional absorption band at $\lambda \approx 380$ nm can be seen, which is assigned by quantum-chemical calculations to the keto species of **3**.

In the steady-state spectrum of **5**, two pronounced absorption bands can be detected with absorption maxima at $\lambda = 351$ and 433 nm. Whereas the former band results from the $\pi\pi^*$ transition, the intense band at $\lambda = 433$ nm overlaps with the $n\pi^*$ band. In addition to the considerable intensity at $\lambda =$ 433 nm, the two bands at $\lambda = 351$ and 433 nm are highly reactive to changes in temperature; this results in different ratios of these bands. At room temperature the ratio is $A_{351/433} = 3.3$

(≈14% keto), whereas it increases slightly to 3.7 at 4 °C and drastically decreases to 1.8 at 80 °C. Therefore, there is an equilibrium between the two species (keto and enol), which is highly affected by temperature (see Figure S13 in the Supporting Information).

Time-resolved investigations

Time-resolved UV/Vis pump/probe experiments have been performed in the femto- to picosecond timescale for all samples in a solution of PBS/10% DMSO to detect the isomerisation dynamics and influence of the keto species after excitation at $\lambda =$ 320, 360 and 440 nm (see Figure 3, below, for transient absorption spectra of **1** and **2** after excitation at $\lambda = 320$ nm; see Figure 6, below, for transient absorption spectra of **3**–**5** after excitation at $\lambda = 320$ nm; and see Figure 10, below, for transient absorption spectrum of **5** after excitation at $\lambda = 440$ nm; spectra after excitation at $\lambda = 360$ nm are not shown). A summary is given in Table 1.

Table 1. Lifetimes [ps] resulting from global lifetime analysis of time-resolved measurements of compounds **1**–**5** after excitation at $\lambda = 320$ and 440 nm.

Lifetime	λ_{ex} 320 nm					440 nm
	1	**2**	**3**	**4**	**5**	**5**
τ_1	0.40	0.15	0.25	0.24	0.33	0.45
τ_2	1.20	0.76	1.30	1.00	1.85	1.96
τ_3	4.40	4.38	3.90	4.27	5.03	–
τ_4	∞	∞	∞	∞	∞	∞

Sulfasalazine versus acetylated sulfasalazine

Independently of the excitation wavelength, compound **1** shows two instantaneously arising excited-state absorption (ESA) bands at $\lambda = 435$ (ESA_1) and 550 nm (ESA_2), as well as ground-state bleaching (GSB) below $\lambda = 390$ nm with $\lambda_{min} =$ 368 nm (Figure 3).

However, the relative contribution of the ESA band to the transient spectrum exhibits a clear dependence on the excitation wavelength. The dataset can be adequately fitted with four time constants. Their respective spectral contribution is visualised in the DAS in Figure 4. While the lifetime $\tau_1 = 0.40$ ps describes the further increase of the amplitude of ESA_1, a general decrease in a broad positive band between $\lambda = 390$ and 600 nm can also be seen. The lifetimes $\tau_2 = 1.20$ ps and $\tau_3 =$ 4.40 ps describe the relaxation of ESA_1 and ESA_2. The DAS of τ_3 shows a sinusoidal shape with a high fit amplitude that describes not only the decay of ESA_1, but also of the GSB. After about 10 ps, compound **1** has relaxed to the ground state. The spectrum reveals a weak product absorption band (PA) at $\lambda =$ 470 nm and a GSB below $\lambda = 445$ nm. The band of the GSB is redshifted with respect to the absorption maximum of the steady-state spectrum (Figure 3, right panel). This indicates

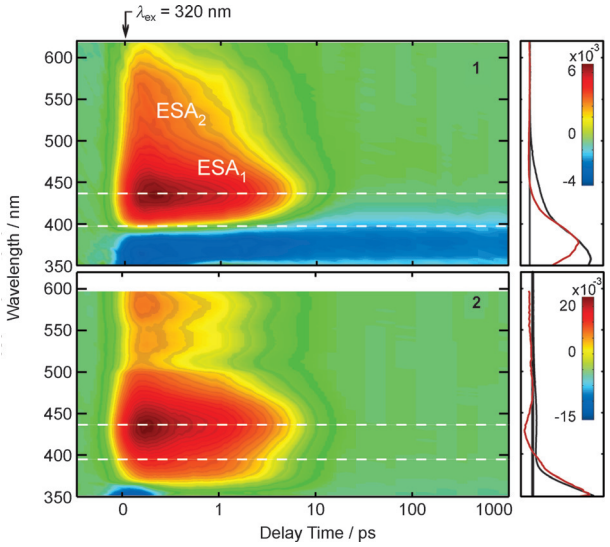

Figure 3. Left: Transient absorption difference spectra of compounds **1** and **2** after excitation at $\lambda = 320$ nm; right: comparison of the absorption spectra before excitation (black) with the transient absorption difference spectrum (red) after 2 ns (inverse decay-associated spectra (DAS) of the longest lifetime). The dashed white lines indicate the wavelengths of the transients shown in Figure 5. As for all transients, the delay time axis is linear for $\tau < 1$ ps and logarithmic for longer delay times.

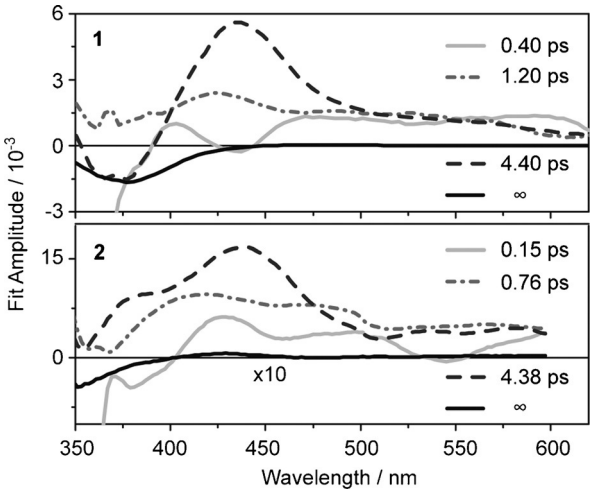

Figure 4. DAS after excitation of compounds **1** and **2** at $\lambda = 320$ nm for the indicated time constants.

a return to the final spectrum beyond the 1 ns timescale, which can be caused by slow conversion reactions.

Because the excitation at $\lambda = 320$ nm induces a transition into the S_2 state of **1**, the broad positive absorption changes at about 100 fs correspond to the $S_2 \rightarrow S_n$ ESA. With a lifetime of 0.40 ps, an ultrafast $S_2 \rightarrow S_1$ transition occurs, as indicated by a decrease in the early broad ESA, which is partially compensated for by an increase in the ESA_1 and ESA_2 bands corresponding to $S_1 \rightarrow S_{m,n}$ transitions. The relaxation into the ground state occurs biexponentially with 1.20 and 4.40 ps. After about 10 ps, the (re-)population of the *trans* ground state and the *cis*-**1** ground state, which can be seen as the PA, is

complete (Figure 4). The spectral behaviour further supports the assignment that the lifetime τ_3 describes the internal conversion into the ground state. Vibrational cooling may contribute; however, no separate lifetime is necessary to describe it. These results correspond well with earlier studies on ABs, for example, nπ*-excited (4-aminomethyl)-phenyl-azobenzoic acid (AMPB),[31–33], known for fast thermal back reactions in aqueous solutions, or ππ* excited push–pull ABs.[34]. Increased longer-lived components have been observed for ABs in organic solvents such as acetonitrile, ethanol or *n*-hexane.[35–37]

Excitation of *trans*-**2** under the same conditions shows roughly comparable spectral and dynamic behaviour. However, the ESA_1 band for **2** is significantly broadened in comparison to that of **1**, due to an additional band at $\lambda = 393$ nm ($A_{393/437} = 0.65$). Contributions at $\lambda = 570$ nm can be observed in addition to the band at $\lambda = 550$ nm, which, however, show the same dynamic features and are therefore considered as a broadened ESA_2 band. The increase of the ESA_1 band for **2** can be seen in the DAS of lifetime τ_1, especially for the band at $\lambda = 393$ nm and only slightly at $\lambda = 460$ nm. After about 8 ps, ESA_1 is already relaxed enough to detect the GSB below $\lambda = 361$ nm again. The PA, which can be seen after about 20 ps, is located at $\lambda = 428$ nm and a GSB below $\lambda = 400$ nm is left. These contributions, as well as the blueshifts of about 40 nm with respect to **1**, are in agreement with the steady-state spectra. The PA is more pronounced for **2**, which should mainly be due to the weaker overlap of the GSB with the PA (Figure 4). By comparing the ESA_1 bands of **1** and **2**, the absorbance changes at $\lambda \approx 437$ nm are similar (Figure 5). For **2**, the contribution of the lifetime τ_2 to the excited-state decay is higher than that for **1**, so the absorbance changes faster between 0.5 and 3 ps.

In the transient absorption spectrum (Figure 3), an additional absorption band at $\lambda = 393$ nm can be seen for compound **2**, which seems to be in contrast to **1**; by comparing the transients of **1** and **2** at $\lambda = 393$ nm (Figure 5), however, they show comparable decay kinetics. Therefore, there is also an ESA band for compound **1** with a spectral overlap with its GSB.

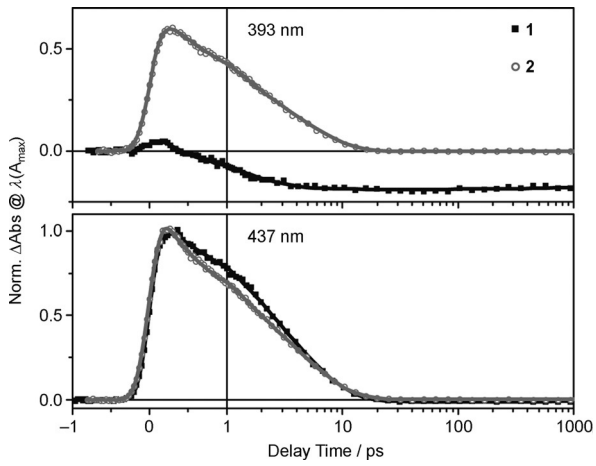

Figure 5. Comparison of transients of compounds **1** and **2** at $\lambda = 393$ and 437 nm normalised at the absorbance maximum of each sample ($\lambda \approx 435$ nm).

Until about 400 fs, a positive signal can be seen in the transients of **1** at $\lambda = 393$ nm, but due to spectral overlap of the GSB with the ESA band, a negative signal results. Because no absorption changes were detected in steady-state spectra, photodeacetylation of **2** during the measurement, and therefore, the excitation of a mixture of **1** and **2** can be excluded.

In summary, significant differences between the $S_0 \rightarrow S_2$ transitions of compounds **1** and **2** could be observed and attributed to their spectral differences. However, they show spectral similarities for the $S_1 \rightarrow S_n$ transitions and comparable dynamics on the sub-nanosecond timescale. Therefore, we suggest a similar electronic structure for the two compounds in the first excited state. Consequently, there is no effect of acetylation on the isomerisation behaviour on the ultrafast timescale.

ortho-/*meta*-/*para*-HO-AB

After excitation of the ππ* band of *trans*-**4** at $\lambda_{ex} = 320$ nm (Figure 6), two instantaneous ESA bands at $\lambda = 393$ (ESA_1) and 510 nm (ESA_2) are induced ($A_{393/510} = 2.9$). Due to the same dynamic features of the contributions at $\lambda = 550$ nm as those at $\lambda = 510$ nm, it is considered as a broadened ESA_2 band. After about 3 ps, ESA_1 has already decayed enough to allow detection of the GSB below $\lambda = 361$ nm. Both ESA bands are com-

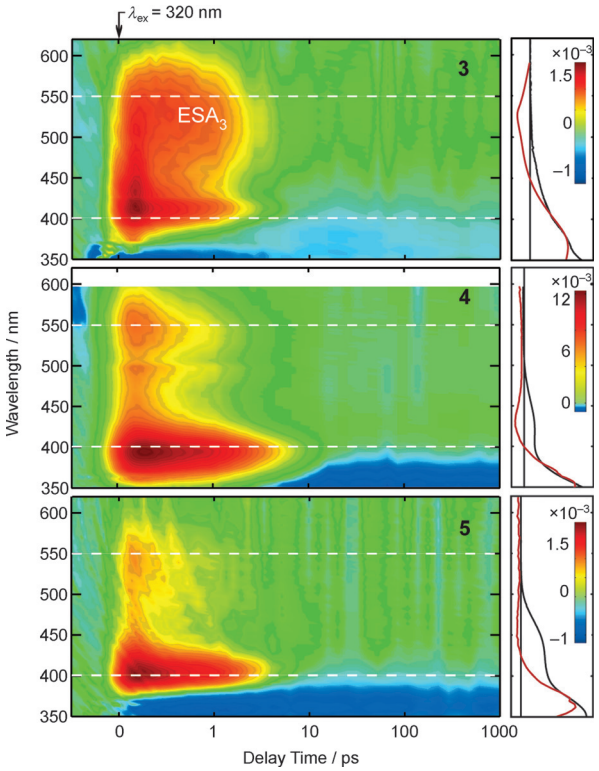

Figure 6. Left: Transient absorption difference spectra of compounds **3**, **4** and **5** after excitation at $\lambda = 320$ nm; right: comparison of the absorption spectra before excitation (black) with the transient absorption difference spectrum (red) after 2 ns (inverse DAS of the longest lifetime); the time slice for **3** is solvent-corrected. The dashed white lines indicate the wavelengths of the transients shown in Figure 8.

pletely relaxed to the ground state after about 15 ps for **4**, and a PA at $\lambda = 430$ nm and GSB below $\lambda = 400$ nm remain.

Excitation of **5** also induces two slightly redshifted ESA bands at $\lambda = 400$ (ESA_1) and 540 nm (ESA_2), with a ratio of $A_{400/540} = 3.1$. Although the ESA_1 band of **5** seems narrower due to spectral overlap with the GSB at $\lambda = 363$ nm, the spectral behaviour is comparable to the isomerisation behaviour of **4**. After about 15 ps, the ESA bands have completely decayed to the ground state and only a GSB below $\lambda = 425$ nm is left, which is slightly redshifted relative to the steady-state spectrum. The PA at $\lambda = 460$ nm is spectrally comparable to that of **1**, yet it is more pronounced. After excitation of **3** at $\lambda = 320$ nm, a GSB signal below $\lambda = 375$ nm and two ESA bands (ESA_1 at $\lambda = 416$ nm and a weaker pronounced band ESA_2 at $\lambda = 510$ nm) arise instantaneously after excitation. In contrast to the other HO-ABs, a third ESA band (ESA_3) between $\lambda = 470$ and 620 nm with $\lambda_{max} = 550$ nm is populated with τ_1: the respective decay associated spectrum (Figure 7) shows a transition from ESA_1 to ESA_3. Therefore, ESA_1 decays with three time constants (τ_1–τ_3), whereas the decay of ESA_2 is described by two time constants (τ_2 and τ_3). The ESA_3 band decays exclusively with a time constant of $\tau_2 = 1.26$ ps. After about 10 ps, ESA_1 and ESA_2 have decayed to the ground state and also the GSB below $\lambda = 365$ nm decreases. However, a second GSB_2 at $\lambda = 380$ nm remains unchanged. Only small changes, barely above the signal-to-noise ratio, can be observed in the range of ESA_3 and the GSB_2 region after 10 ps. One positive PA at $\lambda = 515$ nm remains after decay of the excited-state bands at about 10 ps until at least 1.5 ns, but cannot be seen in flash photolysis measurements beginning at 45 μs. With a lifetime of $\tau = 3.2$ ms, a negative absorption change at $\lambda = 329$ nm decreases (see Figures S11 and S12 in the Supporting Information).

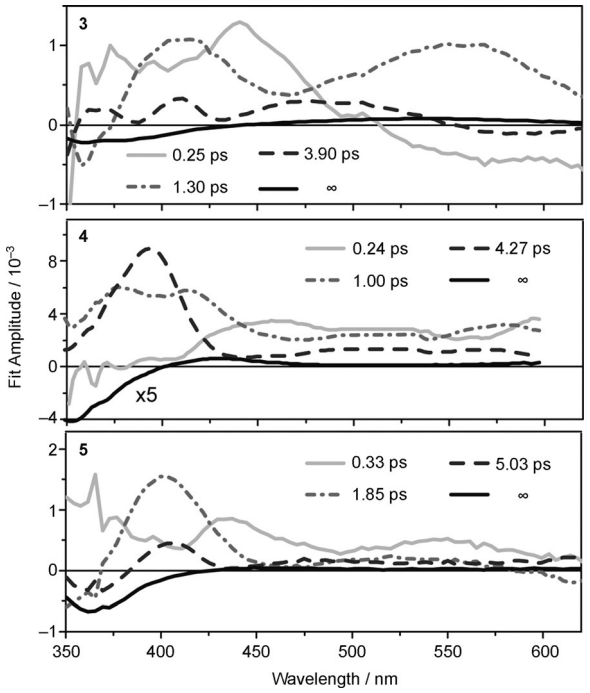

Figure 7. DAS after excitation of compounds **3**, **4** and **5** at $\lambda = 320$ nm corresponding to the indicated time constants.

Similar to **4** and **5**, a fast $S_2 \rightarrow S_1$ transition occurs on a timescale faster than the temporal resolution of the setup, consequently ESA_1 and ESA_2 arise "instantaneously". These bands are assigned to the $S_1 \rightarrow S_n$ transition of *trans*-**3**, which decays biexponentially with τ_2 and τ_3 through a conical intersection back to the *trans*-ground state and the ground state of the *cis* isomer. However, the lifetime τ_1 describes the transition from the ESA_1 band to the S_1 of the keto form (ESA_3), which then decays with τ_2. Therefore, either an excited-state intramolecular proton transfer (ESIPT) occurs from the hydroxyl group (enol) to the nitrogen of the azo group (keto), resulting in a hydrazone structure, or a $S_2 \rightarrow S_1$ transition of the keto-**3** takes place. For the latter possibility, an ESA of the S_2 state would need to overlap with the ESA band of enol-**3**, for which there is no indication. Although, regarding GSB_2, not only was *trans*-**3** excited, but also the keto form; this is in agreement with results from theoretical calculations, which indicate the coexistence of both species in the ground state. This results in ESA_3 in the first place, which is then enhanced by the $ESA_1 \rightarrow ESA_3$ transition (Figure 8).

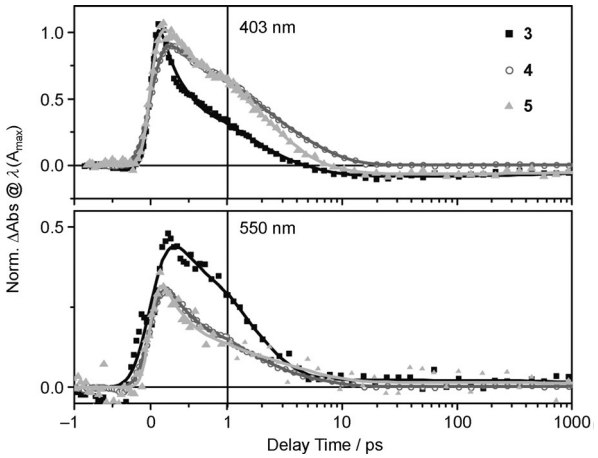

Figure 8. Comparison of transients of compounds **3**, **4** and **5** at $\lambda = 403$ and 550 nm, normalised at the absorbance maximum of each sample ($\lambda \approx 400$ nm); solvent correction for **3** was performed as described in the Experimental Section.

Although for excitation at $\lambda_{ex} = 320$ nm the ratio of $A_{410/550}$ is 1.9 and slightly smaller for $\lambda_{ex} = 440$ nm (1.3), at which the nπ* band is excited, for $\lambda_{ex} = 360$ nm the ESA_3 band is more pronounced (< 1.0) due to increased direct keto- or decreased *trans*-**3** excitation.

The transients of **4** and **5** at $\lambda = 403$ and 500 nm (Figure 8) show similar dynamics. Until about 2 ps, nearly no differences can be observed, but afterwards **5** relaxes slightly slower. However, compound **3** differs not only in the contributions of ESA_1, but also in the $ESA_{2/3}$ bands. At $\lambda = 403$ nm, the positive absorption change decays significantly faster with a pronounced

component on the 100 fs timescale. Nevertheless, complete relaxation to the ground state occurs on a comparable timescale (≈10 ps) as those for **4** and **5**. At $\lambda = 550$ nm, a slight increase in the positive signal can be seen before 350 fs, whereas **4** and **5** gain full intensity after 180 fs. Moreover, compound **3** exhibits a significantly higher intensity, which already reduces below a delay time of 1 ps. After that time, the decay is very steep and remains unchanged after about 6 ps, leaving a small positive signal. This positive absorption arises, on one hand, from *trans–cis* isomerisation, showing the nπ* band of the *cis*-**3**, whereas, on the other hand, it results from an additional pathway via the keto form and can either be assigned to keto-**3** (*trans*- (TK) or *cis*-keto (CK)) in the ground or a triplet states, due to its redshift and longevity, or alternatively to the nπ* band of *cis*-**3**. However, due to the spectral proximity of the isomers involved, a statement about the product of the additional pathway cannot be made unambiguously.

Consequently, isomerisation behaviour similar to that of unsubstituted AB could be observed for compounds **4** and **5**, whereas compound **3** showed an additional excited-state band at $\lambda = 550$ nm, which was attributed to the keto species. This state is populated by the enol species with a lifetime of 250 fs, which corresponds to an ESIPT process. Additionally, isomerisation to *cis*-**3** occurs, due to additional deactivation paths; however, its efficiency is reduced.

According to experimental observations, the photochemical activity of **3** is not dependent on the polarity of the solvent. Very similar spectroscopic signals are measured in different solvents, such as DMSO or water. Apart from *trans–cis* isomerisation and other geometrical deformations in AB derivatives, ESIPT is a well-known deactivation mechanism for many photochromic species. Because the *ortho* substitution of the hydroxy group allows an ESIPT process without participation of solvent molecules, we consider the O_1–H_1 distance to be one of the most relevant coordinates for understanding the photochemistry of compound **3**.

Exploration of the electronic ground state (S_0) at the DFT level leads to a planar *trans*-enol (TE) conformation of **3** as the most stable tautomer. The corresponding TK tautomer lies only 0.1 eV above TE, separated by an energy barrier of 0.2 eV. This indicates that both species might coexist in solution. The *trans–cis* isomerisation around the C_2-N_1-N_2-C_3 bond of the TE species requires surmounting an energy barrier of 2 eV, resulting in a *cis*-enol (CE) conformation that is 0.9 eV higher in energy than that of TE. Conversely, *trans–cis* isomerisation of the keto tautomers involves a somewhat lower barrier (1.4 eV) and leads to a CK form at 0.8 eV above TK. In addition, we have explored internal rotation around the N_2-N_1-C_2-C_1 dihedral angle, following a procedure reported by Cui et al.,[38] in search of additional deactivation paths between the ground and excited electronic states, leading to an alternate TK species (labelled as TK1), 0.4 eV above TK, with an energy barrier of 1.6 eV. These results are summarised in Figure 9a–d. Turning to the S_1 and S_2 potential surfaces calculated by TD-DFT (Figure 9b), in S_1, TE is separated from TK by an energy barrier of 0.3 eV. In S_2, there is no energy minimum for TE, which suggests a barrier-less process starting from the S_2 Franck–Condon geometry. As illustrated in Figure 9a and b, two deactivation pathways can be envisaged,

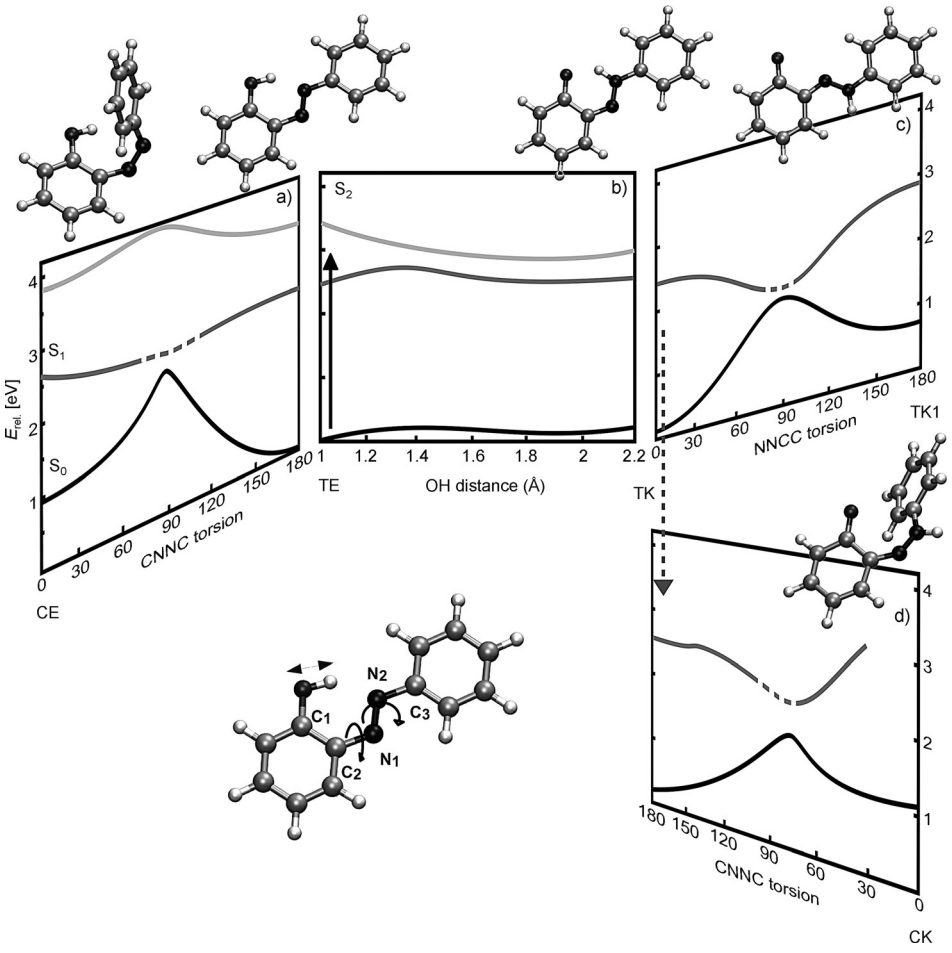

Figure 9. Photochemical landscape of **3**, as inferred from our TD-DFT results. Energies (in eV) in the ground state (S_0, in black), first singlet excited state (S_1, in dark grey) and second singlet excited state (S_2, in light grey) are referenced to the TE minimum in S_0. Energy profiles in S_0 and S_1 are fully relaxed along the corresponding reaction coordinate, whereas the energy profile in S_2 corresponds to vertical energies from S_1. The grey dashed arrow indicates connecting points between panels b) and d). The black arrow corresponds to the starting photoexcitation (Franck–Condon) point of **3**. Dashed lines indicate interpolation in non-adiabatic coupling regions that cannot be described by TD-DFT.

namely, ESIPT (TE–TK conversion) and *trans–cis* isomerisation in the enol form (TE–CE conversion). ESIPT is favoured by the proximity of the S_1 and S_2 PESs, which run parallel to each other along the proton transfer coordinate, showing an energy gap of <0.1 eV. This is indicative of an efficient, ultrafast deactivation path between S_2 and S_1. By contrast, the PES cut along the *trans–cis* isomerisation coordinate (Figure 9a) shows an S_2 barrier of 0.6 eV and an S_2–S_1 energy gap of around 1.0 eV (which could decrease if additional coordinates, leading to an S_1–S_2 conical intersection, were included). Transitions between S_1 and S_0 are seen to be mediated by the torsional coordinates C_2-N_1-N_2-C_3 and N_2-N_1-C_2-C_1 (Figure 9a, c, and d). Assuming that TE–TK conversion is favoured in the initial S_2–S_1 dynamics (see above), subsequent *trans–cis* isomerisation of the TK species encounters an energy gap of 0.6 eV between S_1 and S_0 (Figure 9d), whereas torsion around the N_1-N_2-C_2-C_3 angle results in a smaller gap of 0.3 eV (Figure 9c). In combination, these two torsional coordinates could indicate a hula-twist mechanism.[39] Although TD-DFT is not able to provide a reliable description of the non-adiabatic coupling region, and specifically of the conical intersection topology,[40] related studies have shown that a qualitatively correct picture can be obtained for the photochemical pathway leading on the S_1 state towards the intersection, and its continuation on the S_0 state.[41–43] The energy gap of 0.3 eV is small enough to consider the presence of a conical intersection between these two states, and therefore, an ultrafast and efficient deactivation path.

From the above discussion, the overall scenario of the photochemistry of **3** would involve the following sequence of events: initial excitation of the TE tautomer to S_2 is likely to be followed by ultrafast ESIPT on the coupled S_2 and S_1 surfaces, generating the TK species on S_1 (Figure 9b). Although *trans–cis* isomerisation of the TE species through S_2–S_1–S_0 cannot be excluded, this path is energetically less favoured (Figure 9a). Next, the TK species undergoes passage from S_1 to S_0 through the CNNC and/or NNCC torsional coordinates (Figure 9c and d), presumably leading to a mixture of CK and TK species. The latter is more stable by 0.8 eV than the former.

As mentioned above, the TK species can easily revert to the initial TE reactant by enol/keto tautomerism in S_0; thus closing the photocycle, as observed experimentally. Conversely, the initial photoexcited state should more accurately be described as a mixture of TE and TK, and the above discussion can be straightforwardly adapted to that perspective.

Excitation wavelength dependence of *para*-HO-AB

Although wavelength-dependent excitation of **1** and **3** showed mainly differences in the intensity of the absorbance changes in the ESA band at $\lambda \approx 550$ nm, excitation of compound **5** at $\lambda_{ex} = 440$ nm leads to completely different behaviour than that with $\lambda_{ex} = 320$ nm (Figure 10).

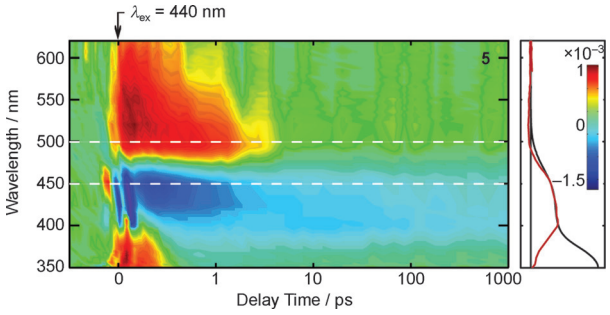

Figure 10. Left: Transient absorption difference spectrum of compound **5** after excitation at $\lambda = 440$ nm; right: comparison of the absorption spectrum before excitation (black) with the transient absorption spectrum (red) after 2 ns (inverse DAS of longest lifetime). The dashed white lines indicate the wavelengths of the transients shown in Figure 11.

Excitation at $\lambda_{ex} = 440$ nm clearly addresses a different absorption band (Figure 2). Instantaneously, after excitation, three ESA bands arise at $\lambda = 383$ nm (ESA_1) and above $\lambda = 480$ nm, at which two ESA bands can be distinguished at $\lambda = 510$ nm (ESA_2) and a less pronounced band at $\lambda = 570$ nm (ESA_3). Although ESA_1 and ESA_3 decay quickly with a lifetime of τ_1, the decays of the GSB ESA_2 occur on a longer timescale. With a lifetime of τ_2, a decrease in the GSB band below $\lambda = 400$ nm and at $\lambda = 452$ nm is described, in addition to the decay of the ESA_2 band and a positive signal at $\lambda = 400$ nm, which is, however, overlaid by the negative signals. After about 10 ps, the excited states have completely decayed to the ground state and leave a positive absorption band at $\lambda = 510$ nm and a GSB below $\lambda = 490$ nm ($\lambda_{min} \approx 430$ nm). The spectral and dynamic characteristics can neither be explained by excitation of *trans*-**5** nor of *cis*-**5**; thus, a different species has to be responsible for this behaviour. Because this species can indeed be seen in the steady-state spectrum (Figure 2), we suggest that **5** is partially present in its keto form, which is not unknown for HO-ABs in protic solvents.[27]

Therefore, at $\lambda = 440$ nm, predominantly keto-**5** is excited and results in a GSB and ESA band at $\lambda = 510$ nm (which corresponds to the $S_1 \rightarrow S_n$ transition). However, this cannot explain ESA_1 and ESA_3, which we attribute to an additional minor excitation of *trans*-**5** in the $n\pi^*$ band (Figure 11). Due to the low extinction coefficient of the $n\pi^*$ band, the dynamics of the

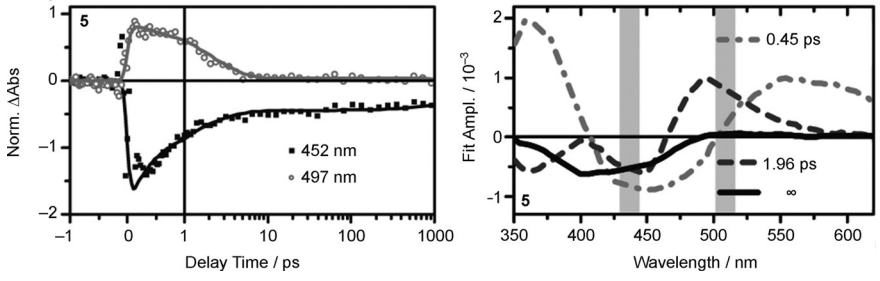

Figure 11. Comparison of transients of compound **5** at $\lambda = 452$ and 497 nm (left) and DAS of **5** (right) after excitation at $\lambda = 440$ nm.

keto species dominate. Nevertheless, *trans–cis* isomerisation does occur. The resulting *cis*-nπ^* band at $\lambda = 510$ nm, however, is too intense, relative to the small GSB of *trans*-**5** at $\lambda = 358$ nm (DAS(τ_4): for $\lambda_{ex} = 440$ nm: $A_{520/361} = 0.47$; for $\lambda_{ex} = 320$ nm: $A_{520/361} = 0.03$), so we propose additional formation of the *cis*-**5** isomer (CE or CK) from the excited keto form through a conical intersection with lifetime τ_2.

In summary, it is possible to address both species of compound **5** (keto and enol) independently by changing the excitation wavelength. Because at room temperature there is still 86% enol species, excitation at $\lambda = 440$ nm results in a mixture of excitation of the keto ($\pi\pi^*$ band) and enol (nπ^* band). It should be noted that, by changing the temperature, however, the thermal equilibrium, and therefore, ratio of excited keto and enol species can be shifted significantly (Figure S13 in the Supporting Information).

As opposed to compound **3**, the photochemistry of compound **5** is strongly dependent on the physical properties of the solvent. Whereas the isomerisation of **5** is observable on a timescale of seconds in DMSO, no conversion can be detected in water on that timescale due to a fast back reaction. Hence, the solvent is expected to play a key role in the deactivation paths of compound **5**. Although the *para* substitution of the hydroxy group rules out an ESIPT process, an intermolecular proton transfer process mediated by solvent molecules is possible. To model this scenario, we have included two types of models in our electronic structure calculations of **5**: The first model includes a chain of seven water molecules that connect the azo bond with the hydroxy group of AB (Figure 12B). The second, simpler model includes two water molecules at a hydrogen-bonding distance to the azo and hydroxy groups, respectively. The first water model was used to identify possible proton transfer along the water chain from the hydroxy group to the azo group through a concerted mechanism. In these models, the optimised ground-state structure again has a planar form for TE and TK, of which TE is slightly more stable than TK by 0.1 eV.

For **5**, the barrier between **5**-TE and **5**-TK strongly depends on the solvent. For the simple water chain model shown in Figure 12, proton transfer across the chain is feasible, but in-

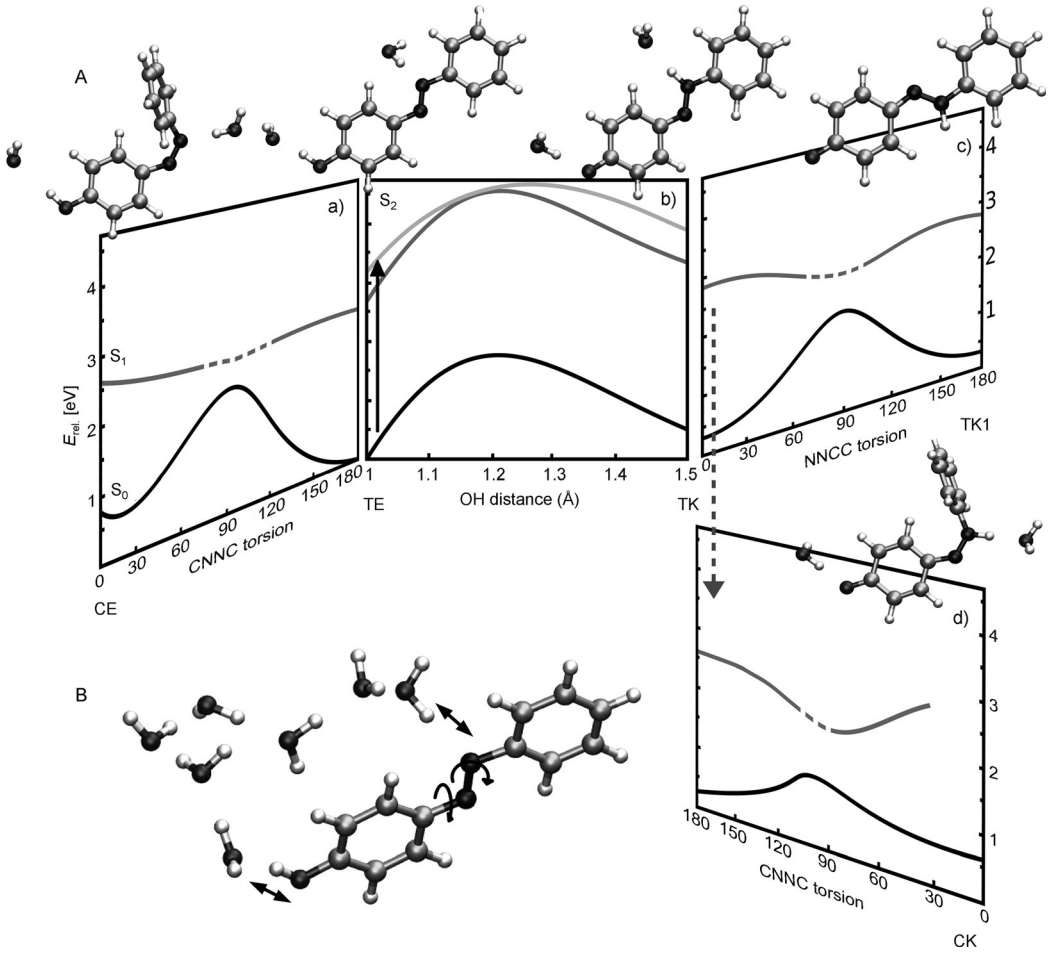

Figure 12. A) Photochemical landscape of compound **5**, as inferred from our electronic structure results. Energies (in eV) in the ground state (S_0, in black), first singlet excited state (S_1, in dark grey) and second singlet excited state (S_2, in light grey) are referenced to the TE minimum in S_0. Energy profiles in S_0 and S_1 are fully relaxed along the corresponding reaction coordinate, whereas the energy profile in S_2 corresponds to vertical energies from S_1. The grey dashed arrow indicates connecting points between panels a)–d). The black arrow indicates the starting photoexcitation (Franck–Condon) point of **5**. As in Figure 9, dashed lines indicate interpolation in non-adiabatic coupling regions that cannot be described by TD-DFT. B) The reaction coordinates for **5** and the water chain model.

volves an artificially high barrier of about 2 eV (Figure 12 b). This barrier could be overcome by supportive O–H frequencies (see Figure S14 in the Supporting Information). Frequency calculations for S_0, S_1 and S_2 show a marked interplay of modes involving water molecules and the azo and hydroxy groups; this supports possible proton transfer from the hydroxy group to the azo group through the water chain. The relevant frequencies are around 3000 to 3500 cm^{-1} (0.3–0.5 eV) for S_0 and can be accessed by participation of the first solvent shell (see Figure S13 in the Supporting Information). The *trans–cis* isomerisation of TE in the S_0 ground state is hindered by a high barrier of about 1.9 eV, leading to a stable CE conformer at 0.6 eV. The *trans–cis* isomerisation of the TK form exhibits a lower barrier of around 0.9 eV, leading to the CK conformation at 0.5 eV. The reverse *cis–trans* isomerisation therefore has a reduced barrier of around 0.4 eV. Internal rotation around the N_2-N_1-C_2-C_1 dihedral angle is also a possible pathway for **5**-TK, with a barrier height of 1.4 eV, which is lower than that for **3**-TK. For S_2 and S_1, TD-DFT calculations also show a high barrier between TE and TK, although this is somewhat reduced compared with the ground state. Possible state crossing between S_2 and S_1 indicates that solvent-mediated passage to S_1 through proton transfer is, in principle, feasible. On the S_1 PES, *trans–cis* isomerisation proceeds in a similar fashion for the TK and TE forms, possibly involving participation of the NNCC torsion, as discussed above.

Deactivation pathway of 5

Following photoexcitation to S_2, compound **5**-TE preferentially decays by *trans–cis* isomerisation to CE (Figure 12A a), due to the high barrier of competing enol/keto tautomerism (Figure 12A b). As mentioned above, this barrier might be significantly lowered, though, in an improved electronic structure description, such that both isomerisation and tautomerism would be feasible.

Likewise, a photoexcited **5**-TK species would preferentially adopt the *trans–cis* isomerisation channel towards CK (see Figure 12A d). Alternatively, the N_2-N_1-C_2-C_1 torsion is feasible (see Figure 12A c). In the electronic ground state (S_0), the barrier for CK-TK back transfer is lower than that of the tautomerism barrier.

Conclusion

In the search for a photoswitchable riboswitch ligand, we realised that the commercially available antipyretic sulfasalazine (**1**) showed no apparent photoswitching behaviour in PBS. In anhydrous DMSO photoswitching can be achieved. However, this effect is prevented by the addition of only 4% PBS to this solution.

Acetylation (to form **2**) afforded a photoswitchable derivative in PBS. This observation suggested that (photo)tautomerism might be the reason for this behaviour. In pump–probe experiments on the ultrafast timescale, we found no significant difference in the time-dependent behaviour of compounds **1** and **2**, which showed that the relevant processes must have occurred on a longer timescale than 2 ns. We confirmed that sulfasalazine in the ground state was present predominantly as the tautomer shown in Figure 1. After photoexcitation, tautomerism in which the resulting keto form had an N–N single bond occurred to a significant degree, leading to fast relaxation to the TE ground state.

To investigate this effect further, we performed a comparative study on the three HO-ABs **3**, **4** and **5** and revealed molecular details of their photodynamics (Figure 13). The influence of the hydroxy group is highly position specific and modulates the individual PESs differently. The *meta*-substituted derivative **4** showed typical AB-like photochemical behaviour due to the absence of prominent tautomerism pathways. The *cis* isomer was stable for several hours. The *ortho*-substituted derivative **3** reacted along two pathways upon excitation: Part of the ensemble of molecules showed normal AB photochemistry with a thermal back reaction to the TE ground state after 3 ms. Because the two additional reaction coordinates (C_2-N_1-N_2-C_3 and N_2-N_1-C_2-C_1), resulting in TK and TK1, showed only small energy differences between S_1 and S_0, this could enable isomerisation through a hula-twist mechanism for *ortho* substitution. Anoth-

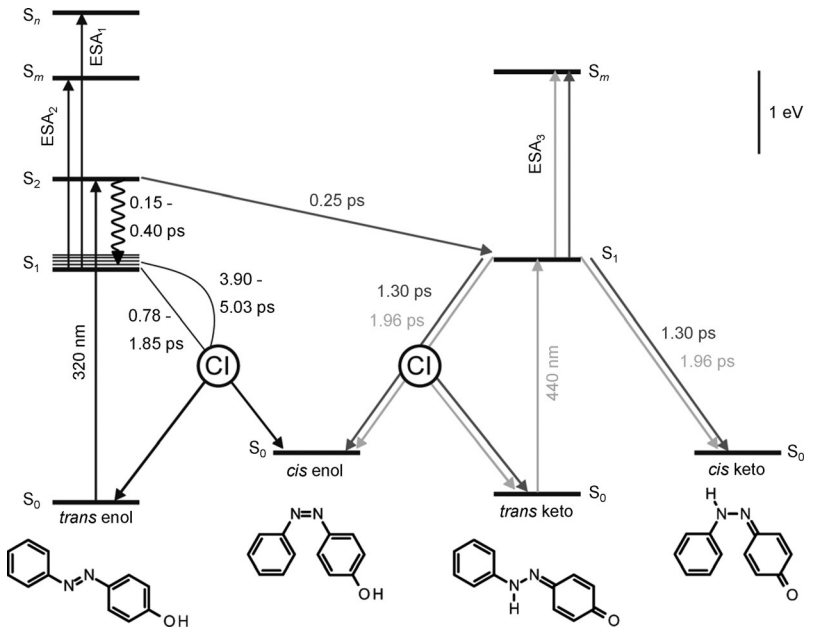

Figure 13. Reaction pathways of HO-ABs in a simplified potential energy scheme. Black arrows indicate the isomerisation mechanism of compounds **1**–**5**. Grey arrows show additional pathways for **3** (dark) and **5** (light). Chemical structures of the respective species are shown for **5** as an example (bottom).

er deactivation pathway through *trans–cis* isomerisation along the CNNC torsion on the S_1 state was suggested. The other part of the excited ensemble performed tautomerism in about 250 fs by OH bond stretching ($\approx$0.3 Å) and then relaxation to the ground state in 10 ps. The behaviour of *para*-substituted compound **5** (which cannot tautomerise intramolecularly) was more complex: In the ground state, a temperature-dependent equilibrium of keto and enol species could be observed, as supported by theoretical calculations; hence, these two species could be selectively excited. Excitation of the enol form again afforded AB-like behaviour with relaxation to the *trans* form within milliseconds. Excitation of the keto form, however, resulted in completely different photochemistry; the transient absorption spectrum reflected the conversion of the excited keto-**5** into the *cis* form.

ABs are important photoswitches that have now been used for several decades to control many important processes in chemical biology and material sciences with light. Knowledge of the pitfalls by a deeper mechanistic understanding of this system will help to make this endeavour an even greater success. With this study, we wanted to contribute to the understanding of why certain AB show no apparent switching on the timescale of seconds and suggest that, for example, simple acetylation can afford photoswitching complex AB derivatives, which could then be good candidates for the development of the corresponding aptamer and later a light-responsive riboswitch.

Experimental Section

Sample preparation

Compounds **2**, **3**, **4**, **5** were prepared by using reported procedures. For comparability, all samples were dissolved in DMSO and diluted with PBS (pH 7.4) to a content of 10% DMSO (ROTIPURAN $\geq$99.8%, p.a.) in solution. Although most of the samples are soluble to an acceptable level, DMSO addition was necessary for the solubility of **3**. For steady-state measurements, about 50 nmol (35 μM, 1.5 mL) was necessary and for flash photolysis about 5 nmol (35 μM, 150 μL) was necessary, whereas for time-resolved studies 90 nmol (350 μM, 250 μL) was used, except for **3**. Due to its low solubility in water, only 12.5 nmol (50 μM, 250 μL) could be prepared for **3**. Steady-state measurements were performed in a 1×1 cm quartz fluorescence cuvette equipped with a 4 mm stirring bar, which allowed simultaneous illumination during measurements. Time-resolved measurements were performed in a 1 mm quartz cuvette. For flash photolysis experiments, a 1×0.2 cm quartz fluorescence cuvette was used.

Experimental setup

NMR spectra were recorded on Bruker AV 500 MHz spectrometer by using [D_6]DMSO as a solvent. HRMS spectra were recorded by using a Thermo Scientific MALDI LTQ Orbitrap instrument.

Steady-state absorption measurements

Absorption spectra were recorded by using a Specord S100 UV/Vis spectrometer. Temperature-dependent absorption spectra were recorded by using a Specord S600 instrument with a Peltier cooled cell holder with stirrer and external heat exchange.

Illumination procedure

For the illumination of the HO-ABs, a Thorlabs light-emitting diode (LED) Driver DC4100 and DC4100-HUB was used. UV light for *trans–cis* isomerisation was provided by a $\lambda = 365$ nm LED and visible light for *cis–trans* isomerisation by a $\lambda = 420$ nm LED (Thorlabs M365L2 and M420L2, 300 mW).

Time-resolved UV/Vis pump–probe setup

Time-resolved measurements were performed in a self-built UV/Vis pump–probe setup. For the generation of ultrashort laser pulses (150 fs), a Ti:sapphire femtosecond laser system from Clark, MXR-CPA-2001, was used with a central wavelength of $\lambda = 775$ nm and a repetition rate of 1 kHz. Excitation pulses were generated in a non-collinear optical parametric amplifier (NOPA) and a subsequent sum frequency mixing process. For an excitation wavelength of $\lambda = 320$ nm, pulses with a wavelength of $\lambda = 545$ nm were mixed with a $\lambda = 775$ nm fundamental pulse in a BBO crystal ($\theta = 36^\circ$); for $\lambda_{max} = 360$ nm a NOPA pulse of $\lambda = 672$ nm and a $\theta = 30.2^\circ$ BBO crystal were used and for $\lambda_{max} = 440$ nm a NOPA pulse of 1018 nm and a $\theta = 26^\circ$ BBO crystal were used, resulting in an energy of about 50 nJ. For the probe pulse, a fundamental pulse was guided into a 5 mm CaF_2 window to generate white light, which was focused together with the excitation pulse into the sample. Polarisation between the pump and probe pulse was adjusted to an angle of 54.7° between the two pulses to eliminate anisotropic effects. The cuvette was rotated in the *x,y* plane and illuminated by a $\lambda =$ 420 nm LED during measurements to provide the initial state of the sample. The averaged temporal resolution was in the range of about 220 fs. Difference spectra were calculated by blocking every second excitation pulse. Transient absorption data were analysed by global lifetime analysis (GLA)[44] by using up to four exponential functions. The coherent artefact contribution around time zero was approximated with a Gaussian function and its first and second derivatives.[45] The analysis was performed by using OPTIMUS.[46]. Time-resolved spectra were solvent-corrected by subtracting the scaled transient data of the solvent.

Flash photolysis

An excitation pulse with a wavelength of $\lambda = 320$ nm (pulse width: 20 ns, intensity: 0.7 mJ cm^{-2}) was obtained by second-harmonic generation of the pulses of an optical parametric oscillator (OPO; GWU-Lasertechnik Vertriebsges. mbH), which was pumped by a Nd:YAG laser (Spitfire 600 Innolas Laser GmbH). For broadband detection, a charge-coupled device (CCD) camera (PI-MAX3, Princeton Instruments) and a spectrograph (Acton SP2150, Princeton Instruments) were used. For difference spectra, every second excitation pulse was blocked.

Theoretical calculations

DFT methods were employed to explore the topology of the ground (S_0), first singlet excited (S_1) and second singlet excited (S_2) electronic states. Ground-state DFT calculations were performed in S_0, whereas TD-DFT[47] was used in S_1 and S_2. TD-DFT has been successfully applied to study other related photochromic and ESIPT systems. The three-parameter hybrid functional of Becke with the correlation functional of Lee, Yang and Parr (B3-LYP) has been used.[48,49] The Weigend and Ahlrichs def2-TZVP basis set was con-

sidered,[50] which included polarisation functions for all atoms. All calculations were carried out by using the Gaussian 09 package.[51] For the ground electronic state, the geometries of all stationary points (minima and transition states) were localised upon direct optimisation. In the first excited electronic state, the minima were also directly minimised, whereas the transition states were located as maxima of reaction coordinates. The second singlet excited state was constructed as vertical single-point calculations from the relaxed structures of S_1. For the reaction coordinates, the O_1–H_1 distance was used for the intramolecular proton transfer process in compound **3**, whereas the H_1–O_2 and H_3–N_2 distances were used for compound **5**. For both molecules, the C_2-N_1-N_2-C_3 and N_2-N_1-C_2-C_1 dihedral angles were used for internal rotations (see Figure 9 for atom numbering). The calculations were first carried out for the isolated molecule (gas phase) and later with solvent by using the polarisable continuum model (PCM),[52–54] in which the HO-ABs were placed inside a cavity of implicit water solvent. All optimisations and reaction coordinates were repeated inside the solvent cavity. For compound **5**, explicit water molecules were used, as obtained from a molecular dynamics trajectory of **5** in a cubic box of TIP3P water molecules[55] by using the Amber 10 package[56] and Generalized Amber Force Field.[57]. After 10 ns of equilibration at a constant pressure and temperature of 1 atm and 300 K, respectively, we manually selected the smallest cluster of water molecules that connected the –OH donor and –N acceptor groups of compound **5**. Stationary points were identified through frequency calculations in the ground and first singlet excited electronic states.

Synthesis of 2

Sulfasalazine (0.50 g, 1.26 mmol) was added to acetic anhydride (3 mL) and the reaction mixture was heated for 3 h. The solvent was removed under pressure and the product was isolated by column chromatography (cyclohexane (CH)/ethyl acetate (EE) 1:1) to yield **2** (0.27 g, 0.56 mmol, 45%). ^{1}H NMR (500 MHz, [D_6]DMSO): δ = 13.55 (s, 1H; -COOH), 8.71–8.69 (m, 1H; H_{ar}), 8.46–8.45 (d, J = 2.4 Hz, 1H; H_{ar}), 8.29–8.22 (m, 3H; H_{ar}), 8.16–8.11 (m, 3H; H_{ar}), 7.79–7.78 (d, J = 7.8 Hz, 1H; H_{ar}), 7.66–7.63 (m, 1H; H_{ar}), 7.51–7,49 (d, J = 8.6 Hz, 1H; H_{ar}), 2.31 (s, 3H; -CH_3), 1.81 ppm (s, 3H, -CH_3); ^{13}C NMR (75.5 MHz, [D_6]DMSO): δ = 169.6, 169.0, 164.9, 154.4, 152.8, 150.0, 149.4, 149.2, 140.2, 139.8, 130.1, 128.1, 126.0, 125.50, 125.45, 125.43, 125.3, 123.0, 24.4, 20.8 ppm; HRMS (MALDI): *m/z* calcd for $C_{22}H_{18}N_4O_7SK$ $[M+K]^+$: 521.05278; found: 521.05222 (Δm 0.00056, error 0.11 ppm).

Synthesis of 3

Nitrosobenzene (0.50 g, 4.67 mmol) was dissolved in acetic acid (30 mL). 2-Aminophenol (0.51 g, 4.67 mmol) was added to the green solution and the mixture was stirred for 24 h under an argon atmosphere. The solvent was removed under reduced pressure and the product was isolated by column chromatography (CH/EE 40:1) to yield **3** (0.47 g, 2.39 mmol, 51%). ^{1}H NMR (500 MHz, [D_6]DMSO): δ = 11.18 (s, 1H; -OH), 7.99–7.97 (m, 2H; H_{ar}), 7.77–7.75 (dd, J = 8.05, 1H; H_{ar}), 7.61–7.55 (m, 3H; H_{ar}), 7.44–7.41 (m, 1H; H_{ar}), 7.08–7.06 (m, 1H; H_{ar}), 7.03–6.99 ppm (m, 1H; H_{ar}); ^{13}C NMR (125.8 MHz, [D_6]DMSO): δ = 154.4, 151.4, 138.3, 133.6, 131.3, 129.4, 123.2, 122.6, 119.8, 118.2 ppm; HRMS (MALDI): *m/z* calcd for $C_{12}H_{10}N_2O$ $[M]^+$: 199.08659; found: 199.08654 (Δm 0.00005, error 0.25 ppm).

Synthesis of 4

Nitrosobenzene (0.50 g, 4.67 mmol) was dissolved in acetic acid (30 mL). 3-Aminophenol (0.51 g, 4.67 mmol) was added to the green solution and the mixture was stirred for 24 h under an argon atmosphere. The solvent was removed under pressure and the product was isolated by column chromatography (CH/EE 9:1) to yield **4** (0.67 g, 3.41 mmol, 73%). ^{1}H NMR (500 MHz, [D_6]DMSO): δ = 9.87 (s, 1H; -OH), 7.88–7.86 (m, 2H; H_{ar}), 7.60–7.55 (m, 3H; H_{ar}), 7.40–7.39 (m, 2H; H_{ar}), 7.27–7.26 (m, 1H; H_{ar}), 6.99–6.96 ppm (m, 1H; H_{ar}); ^{13}C NMR (125.8 MHz, [D_6]DMSO): δ = 158.3, 153.2, 151.9, 131.5, 130.2, 129.5, 122.5, 118.8, 115.5, 107.2 ppm; HRMS (MALDI): *m/z* calcd for $C_{12}H_{10}N_2O$ $[M]^+$: 199.08659; found: 199.08651 (Δm 0.00008, error 0.40 ppm).

Synthesis of 5

Nitrosobenzene (0.50 g, 4.67 mmol) was dissolved in acetic acid (30 mL). 4-Aminophenol (0.51 g, 4.67 mmol) was added to the green solution and the mixture was stirred for 24 h under an argon atmosphere. The solvent was removed under pressure and the product was isolated by column chromatography (CH/EE 9:1) to yield **5** (0.73 g, 3.69 mmol, 79%). ^{1}H NMR (500 MHz, [D_6]DMSO): δ = 10.31 (s, 1H; -OH), 7.82–7.80 (m, 4H; H_{ar}), 7.57–7.54 (m, 2H; H_{ar}), 7.50–7.49 (m, 1H; H_{ar}), 6.96–6.94 ppm (m, 2H; H_{ar}); ^{13}C NMR (125.8 MHz, [D_6]DMSO): δ = 161.0, 152.1, 145.2, 130.5, 129.3, 124.9, 122.1, 115.9 ppm; HRMS (MALDI): *m/z* calcd for $C_{12}H_{10}N_2O$ $[M]^+$: 199.08659; found: 199.08667 (Δm 0.00008, error 0.40 ppm).

Acknowledgements

We thank the Deutsche Forschungsgemeinschaft (DFG) for financial support through SFB 902 "Molecular Principles of RNA-Based Regulation".

Keywords: azobenzenes · tautomerism · photochemistry · time-resolved spectroscopy · water chemistry

[1] W. Szymański, J. M. Beierle, H. A. V. Kistemaker, W. A. Velema, B. L. Feringa, *Chem. Rev.* **2013**, *113*, 6114–6178.
[2] C. Brieke, F. Rohrbach, A. Gottschalk, G. Mayer, A. Heckel, *Angew. Chem. Int. Ed.* **2012**, *51*, 8446–8476.
[3] G. Mayer, A. Heckel, *Angew. Chem. Int. Ed.* **2006**, *45*, 4900–4921; *Angew. Chem.* **2006**, *118*, 5020–5042.
[4] Y. Zhao, T. Ikeda, *Smart Light-Responsive Materials: Azobenzene-Containing Polymers and Liquid Crystals*, Wiley, **2009**.
[5] H. M. D. Bandara, S. C. Burdette, *Chem. Soc. Rev.* **2012**, *41*, 1809–1825.
[6] A. A. Beharry, G. A. Woolley, *Chem. Soc. Rev.* **2011**, *40*, 4422–4437.
[7] G. S. Kumar, D. C. Neckers, *Chem. Rev.* **1989**, *89*, 1915–1925.
[8] Z. Yu, S. Hecht, *Angew. Chem. Int. Ed.* **2013**, *52*, 13740–13744.
[9] A. Köhntopp, A. Dabrowski, M. Malicki, F. Temps, *Chem. Commun.* **2014**, *50*, 10105–10107.
[10] S. K. Yesodha, C. K. S. Pillai, N. Tsutsumi, *Prog. Polym. Sci.* **2004**, *29*, 45–74.
[11] J. Wachtveitl, A. Zumbusch, *Chembiochem* **2011**, *12*, 1169–1170.
[12] J. Bredenbeck, J. Helbing, A. Sieg, T. Schrader, W. Zinth, C. Renner, R. Behrendt, L. Moroder, J. Wachtveitl, P. Hamm, *Proc. Natl. Acad. Sci. USA* **2003**, *100*, 6452–6457.
[13] S. Spörlein, H. Carstens, H. Satzger, C. Renner, R. Behrendt, L. Moroder, P. Tavan, W. Zinth, J. Wachtveitl, *Proc. Natl. Acad. Sci. USA* **2002**, *99*, 7998–8002.
[14] U. Kusebauch, S. A. Cadamuro, H.-J. Musiol, M. O. Lenz, J. Wachtveitl, L. Moroder, C. Renner, *Angew. Chem. Int. Ed.* **2006**, *45*, 7015–7018; *Angew. Chem.* **2006**, *118*, 7170–7173.

[15] T. Goldau, K. Murayama, C. Brieke, S. Steinwand, P. Mondal, M. Biswas, I. Burghardt, J. Wachtveitl, H. Asanuma, A. Heckel, *Chem. Eur. J.* **2015**, *21*, 2845 – 2854.
[16] H. Ito, X. Liang, H. Nishioka, H. Asanuma, *Org. Biomol. Chem.* **2010**, *8*, 5519 – 5524.
[17] M. A. Kienzler, A. Reiner, E. Trautman, S. Yoo, D. Trauner, E. Y. Isacoff, *J. Am. Chem. Soc.* **2013**, *135*, 17683 – 17686.
[18] R. H. Kramer, D. L. Fortin, D. Trauner, *Curr. Opin. Neurobiol.* **2009**, *19*, 544 – 552.
[19] N. J. Dunn, W. H. Humphries, A. R. Offenbacher, T. L. King, J. A. Gray, *J. Phys. Chem. A* **2009**, *113*, 13144 – 13151.
[20] J. Dokić, M. Gothe, J. Wirth, M. V. Peters, J. Schwarz, S. Hecht, P. Saalfrank, *J. Phys. Chem. A* **2009**, *113*, 6763 – 6773.
[21] M. Kojima, S. Nebashi, K. Ogawa, N. Kurita, *J. Phys. Org. Chem.* **2005**, *18*, 994 – 1000.
[22] J. Garcia-Amorós, M. Díaz-Lobo, S. Nonell, D. Velasco, *Angew. Chem. Int. Ed.* **2012**, *51*, 12820 – 12823.
[23] J. Garcia-Amorós, A. Sánchez-Ferrer, W. A. Massad, S. Nonell, D. Velasco, *Phys. Chem. Chem. Phys.* **2010**, *12*, 13238 – 13242.
[24] L. Antonov, V. Deneva, S. Simeonov, V. Kurteva, D. Nedeltcheva, J. Wirz, *Angew. Chem. Int. Ed.* **2009**, *48*, 7875 – 7878; *Angew. Chem.* **2009**, *121*, 8015 – 8018.
[25] J.-M. Savéant, C. Tard, *J. Am. Chem. Soc.* **2014**, *136*, 8907 – 8910.
[26] G. Gabor, E. Fischer, *J. Phys. Chem.* **1962**, *66*, 2478 – 2481.
[27] J. García-Amorós, D. Velasco, *Beilstein J. Org. Chem.* **2012**, *8*, 1003 – 1017.
[28] B. R. Hsieh, D. Désilets, P. M. Kazmaier, *Dye. Pigment.* **1990**, *14*, 165 – 189.
[29] M. Sahu, M. B. Saha, S. C. Bera, *Photochem. Photobiol.* **1995**, *89*, 19 – 24.
[30] J. Griffiths, *Chem. Soc. Rev.* **1972**, *1*, 481 – 493.
[31] C. Renner, L. Moroder, *ChemBioChem* **2006**, *7*, 868 – 878.
[32] H. Satzger, C. Root, C. Renner, R. Behrendt, L. Moroder, J. Wachtveitl, W. Zinth, *Chem. Phys. Lett.* **2004**, *396*, 191 – 197.
[33] J. Wachtveitl, S. Spörlein, H. Satzger, B. Fonrobert, C. Renner, R. Behrendt, D. Oesterhelt, L. Moroder, W. Zinth, *Biophys. J.* **2004**, *86*, 2350 – 2362.
[34] J. Bahrenburg, K. Röttger, R. Siewertsen, F. Renth, F. Temps, *Photochem. Photobiol. Sci.* **2012**, *11*, 1210 – 1219.
[35] I. K. Lednev, T.-Q. Ye, R. E. Hester, J. N. Moore, *J. Phys. Chem.* **1996**, *100*, 13338 – 13341.
[36] H. Satzger, C. Root, M. Braun, *J. Phys. Chem. A* **2004**, *108*, 6265 – 6271.
[37] M. Quick, A. L. Dobryakov, M. Gerecke, C. Richter, F. Berndt, I. N. Ioffe, A. A. Granovsky, R. Mahrwald, N. P. Ernsting, S. A. Kovalenko, *J. Phys. Chem. B* **2014**, *118*, 8756 – 8771.
[38] G. Cui, P.-J. Guan, W.-H. Fang, *J. Phys. Chem. A* **2014**, *118*, 4732 – 4739.
[39] D. Sampedro Ruiz, A. Cembran, M. Garavelli, M. Olivucci, W. Fuß, *Photochem. Photobiol.* **2002**, *76*, 622 – 633.
[40] B. G. Levine, C. Ko, J. Quenneville, T. J. Martinez, *Mol. Phys.* **2006**, *104*, 1039 – 1051.
[41] J. M. Ortiz-Sánchez, R. Gelabert, M. Moreno, J. M. Lluch, *J. Chem. Phys.* **2008**, *129*, 21430801 – 21430811.
[42] J. M. Ortiz-Sánchez, R. Gelabert, M. Moreno, J. M. Lluch, J. M. Anglada, J. M. Bofill, *Chem. Eur. J.* **2010**, *16*, 6693 – 6703.
[43] J. M. Ortiz-Sánchez, R. Gelabert, M. Moreno, J. M. Lluch, *ChemPhysChem* **2010**, *11*, 3696 – 3703.
[44] I. H. M. van Stokkum, D. S. Larsen, R. van Grondelle, *Biochim. Biophys. Acta Bioenerg.* **2004**, *1657*, 82 – 104.
[45] S. A. Kovalenko, A. L. Dobryakov, J. Ruthmann, N. P. Ernsting, *Phys. Rev. A* **1999**, *59*, 2369 – 2384.
[46] C. Slavov, H. Hartmann, J. Wachtveitl, *Anal. Chem.* **2015**, *87*, 2328 – 2336.
[47] R. Bauernschmitt, R. Ahlrichs, *Chem. Phys. Lett.* **1996**, *256*, 454 – 464.
[48] A. D. Becke, *J. Chem. Phys.* **1993**, *98*, 5648 – 5652.
[49] C. Lee, W. Yang, R. Parr, *Phys. Rev.* **1988**, *37*, 785 – 789.
[50] F. Weigend, R. Ahlrichs, *Phys. Chem. Chem. Phys.* **2005**, *7*, 3297 – 3305.
[51] M. J. Frisch, G. W. Trucks, H. B. Schlegel, G. E. Scuseria, M. A. Robb, J. R. Cheeseman, J. A. Montgomery, Jr., T. Vreven, K. N. Kudin, J. C. Burant, J. M. Millam, S. S. Iyengar, J. Tomasi, V. Barone, B. Mennucci, M. Cossi, G. Scalmani, N. Rega, G. A. Petersson, H. Nakatsuji, M. Hada, M. Ehara, K. Toyota, R. Fukuda, J. Hasegawa, M. Ishida, T. Nakajima, Y. Honda, O. Kitao, H. Nakai, M. Klene, X. Li, J. E. Knox, H. P. Hratchian, J. B. Cross, V. Bakken, C. Adamo, J. Jaramillo, R. Gomperts, R. E. Stratmann, O. Yazyev, A. J. Austin, R. Cammi, C. Pomelli, J. W. Ochterski, P. Y. Ayala, K. Morokuma, G. A. Voth, P. Salvador, J. J. Dannenberg, V. G. Zakrzewski, S. Dapprich, A. D. Daniels, M. C. Strain, O. Farkas, D. K. Malick, A. D. Rabuck, K. Raghavachari, J. B. Foresman, J. V. Ortiz, Q. Cui, A. G. Baboul, S. Clifford, J. Cioslowski, B. B. Stefanov, G. Liu, A. Liashenko, P. Piskorz, I. Komaromi, R. L. Martin, D. J. Fox, T. Keith, M. A. Al-Laham, C. Y. Peng, A. Nanayakkara, M. Challacombe, P. M. W. Gill, B. Johnson, W. Chen, M. W. Wong, C. Gonzalez, J. A. Pople, Gaussian 09, Revision D.01, Gaussian, Inc., Wallingford CT, **2009**.
[52] S. Miertus, E. Scroco, J. Tomasi, *J. Chem. Phys.* **1981**, *55*, 117 – 129.
[53] R. Improta, V. Barone, G. Scalmani, J. Frisch, *J. Chem. Phys.* **2006**, *125*, 0541031 – 0541039.
[54] R. Improta, G. Scalmani, M. J. Frisch, V. Barone, *J. Chem. Phys.* **2007**, *127*, 07450401 – 07450409.
[55] W. L. Jorgensen, J. Chandrasekhar, J. D. Madura, R. W. Impey, M. L. Klein, *J. Chem. Phys.* **1983**, *79*, 926 – 935.
[56] D. A. Case, T. A. Darden, T. E. Cheatham, III, C. L. Simmerling, J. Wang, R. E. Duke, R. Luo, M. Crowley, R. C. Walker, W. Zhang, K. M. Merz, B. Wang, S. Hayik, A. Roitberg, G. Seabra, I. Kolossváry, K. F. Wong, F. Paesani, J. Vanicek, X. Wu, S. R. Brozell, T. Steinbrecher, H. Gohlke, L. Yang, C. Tan, J. Mongan, V. Hornak, G. Cui, D. H. Mathews, M. G. Seetin, C. Sagui, V. Babin, P. A. Kollman, AMBER 10, University of California, San Francisco, **2010**.
[57] J. Wang, R. M. Wolf, J. W. Caldwell, P. A. Kollman, D. A. Case, *J. Comput. Chem.* **2004**, *25*, 1157 – 1174.

Received: May 12, 2015
Published online on September 8, 2015